Comunicações Geológicas, 2009, t. 96, pp. 83-100

Assumptions and problems with Fe-Mg garnet – biotite diffusion based petrological cooling rates: a case study in granulites and migmatites from central Ribeira Fold Belt, SE Brazil

T. M. Bento dos Santos*[1]; J. M. U. Munhá**; C. C. G. Tassinari*** & P. E. Fonseca**

Keywords: Petrological cooling rates; Fe-Mg diffusion; Ribeira Fold Belt.

Abstract: The São Fidelis – Santo António de Pádua sector of central Ribeira Fold Belt is mainly composed of migmatites, granulites and blastomylonites. Application of two contrasting methodologies to obtain petrological cooling rates based on Fe-Mg diffusion between garnet and respective biotite inclusions proved unfruitful. This was mainly due to: a) high dispersion of results caused by open-system behaviour; and b) narrow closure temperature variation caused by garnet reequilibration at high temperatures followed by very fast cooling. The obtained results are mainly qualitative but in broad agreement with previously obtained thermochronological results based on integration of multiple isotopic systems.

Palavras-chave: Taxas de arrefecimento petrológicas; Difusão Fe-Mg; Faixa Ribeira.

Resumo: O sector São Fidelis – Santo António de Pádua, pertencente à zona central da Faixa Ribeira, é fundamentalmente composto por migmatitos, granulitos e blastomilonitos. A aplicação de diferentes metodologias com o objectivo de obter taxas de arrefecimento baseadas na difusão Fe-Mg entre granada e respectivas inclusões de biotite revelou-se infrutífera. Tal deve-se fundamentalmente a: a) elevada dispersão dos resultados causada pela existência de um sistema aberto; b) estreita variação das temperaturas de fecho do sistema causada por re-homogeneização da granada a altas temperaturas seguida de arrefecimento muito rápido. Os resultados obtidos são fundamentalmente qualitativos, mas estão de acordo com resultados termocronológicos previamente obtidos baseados na integração de múltiplos sistemas isotópicos.

1. INTRODUCTION

Previous works in central Ribeira Fold Belt (RFB) established age constraints for the Brasiliano orogeny and tectonic evolution of the belt (e.g.: Cordani *et al*., 1973; Machado *et al*., 1996; Schmitt *et al*., 2004; 2008; Heilbron & Machado, 2003; Bento dos Santos *et al*., 2007; Fonseca *et al*., 2008). However, there are few thermochronological studies (Bento dos Santos *et al*., 2008; Fonseca *et al*., 2008; Schmitt *et al*., 2004) that accurately depict the geodynamic evolution and quantitatively constrain the cooling rates of central RFB.

This work provides new petrological cooling rates, which can be determined from analysis of diffusional zoning in metamorphic minerals (Spear & Parrish, 1996). Here, petrological cooling rates based on Fe-Mg diffusion between garnet and biotite inclusions for the studied granulites and migmatites are presented. The obtained results are then compared with geochronological cooling rates previously obtained in the study area (Bento dos Santos *et al*., 2008).

Several authors tried to use mineral diffusion mechanisms in order to determine cooling rates (e.g.: Dodson, 1973; Lasaga *et al*., 1977; Ehlers *et al*., 1994; Spear & Parrish, 1996). These authors assumed that diffusion induced by compositional variation in the garnet-biotite interface is a function of $Kd_{(Mg/Fe)}^{Garnet\text{-}Biotite}$ in response to thermal changes, such as cooling during the retrograde path. During cooling garnet is enriched in

* LNEG – Laboratório Nacional de Energia e Geologia, Estrada da Portela – Zambujal – Alfragide, 2720-866 Amadora, Portugal ([1]Corresponding author: telmo.santos@ineti.pt).

** Centro/Departamento de Geologia, Universidade de Lisboa, Edifício C6, 3º, Campo Grande, 1749-016 Lisboa, Portugal. jmmunha@fc.ul.pt; pefonseca@fc.ul.pt.

*** Instituto de Geociências, Universidade de São Paulo, Rua do Lago, 562 – Butantã, CEP: 05508-080, São Paulo, Brazil. ccgtassi@usp.br.

Fe/(Fe+Mg), whereas biotite inclusions become poorer. When temperature drops below closure temperature, diffusion becomes negligible. The diffusive process is limited by the rate of diffusion in garnet, because $D_{Fe/Mg}^{Biotite} >> D_{Fe/Mg}^{Garnet}$ and mass balance determines that diffusive flows (rate of cation transfer in the mineral interface) between garnet and biotite must be the same. Therefore, Fe/(Fe+Mg) variations will be a function of biotite inclusion size or garnet/biotite proportion. This implies that Fe/(Fe+Mg) results in garnet and biotite inclusions can be transformed in its respective apparent closure temperature and cooling rates can be obtained (Fig. 1). The used methodologies only consider diffusion between garnet and respective biotite inclusions and exclude garnet – matrix biotite interface diffusive processes, because it is very likely that the latter had open-system behaviour. Besides, most matrix biotite is affected or was formed by net-transfer reactions that include consumption of garnet rims. Therefore, it is unreasonable to use garnet and matrix biotites to model cation diffusion based petrological cooling rates.

This work explores the referred assumptions that allow petrological cooling rates to be applied to natural systems, as well as the potential pitfalls regarding these methodologies, namely the difficulty in assuring that open-system behaviour did not take place in complex orogenic belts, such as the RFB. Therefore, this article is a critic work to the applied methodologies and also a first attempt to constrain petrological cooling rates in the RFB.

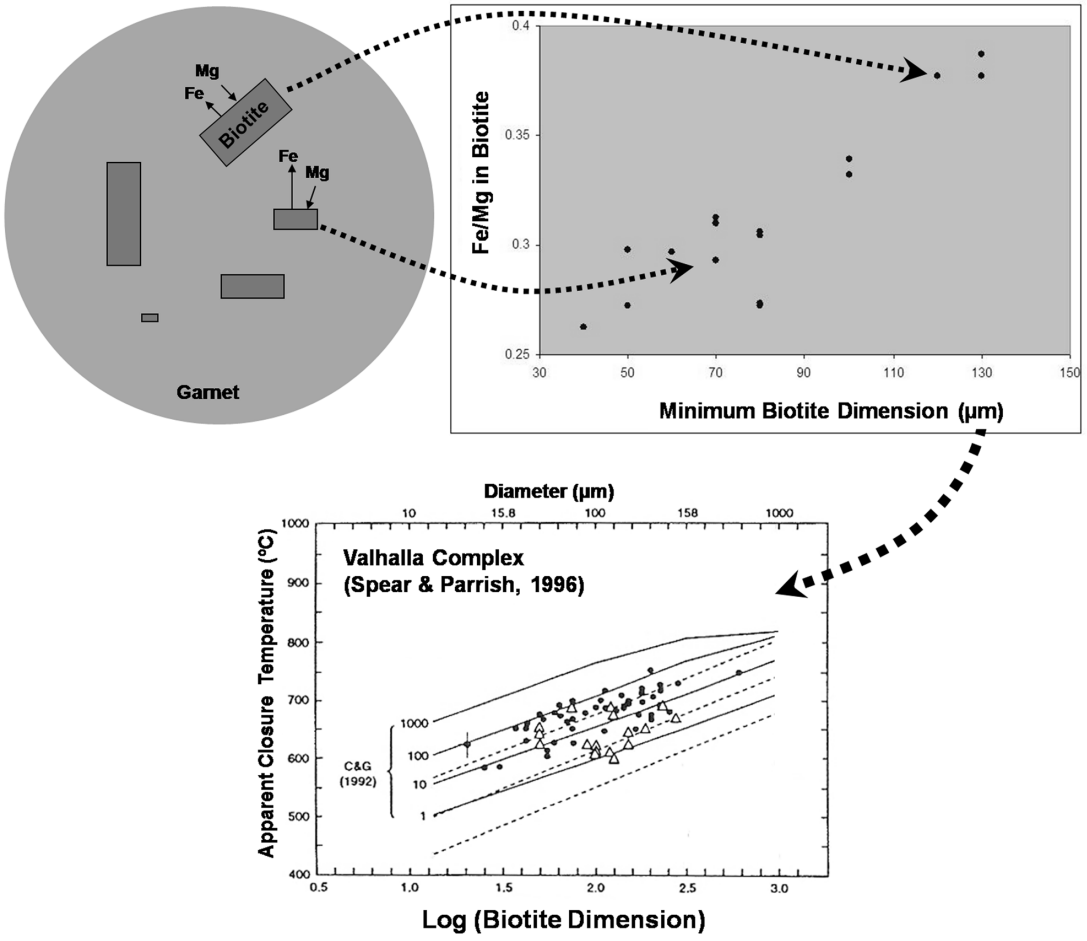

Fig. 1 – Schematics showing how composition of biotite inclusions are dependent of respective size and how their Fe/Mg composition can be transformed in petrological cooling rates using the Spear & Parrish (1996) methodology. Garnet's core composition is used with the Ferry & Spear (1978) thermometer in order to obtain apparent closure temperatures. Chakraborty & Gangully (1992) – C&G (1992) – diffusion coefficients are used to depict the petrological cooling rates. In this example, cooling rates range from 1 – 1000ºC/Ma (modified from Spear & Parrish, 1996).

2. GEOLOGICAL SETTING AND FIELD OBSERVATIONS

The RFB extends over 1,500 km along the SE Brazilian coast from southern Bahia State to Uruguay, through Espírito Santo, Rio de Janeiro, Minas Gerais, São Paulo and Paraná States (CORDANI, 1971). The RFB is a NE-SW trending (south and central sectors) and NNE-SSW trending (northern sector) Neoproterozoic mobile belt (CORDANI *et al*., 1973) formed during the Brasiliano Orogeny as outcome of the collision between the São Francisco and West Congo cratons, from which resulted Western Gondwana at around 670 – 480 Ma ago (TROUW *et. al*., 2000; SCHMITT *et al*., 2008) (Fig. 2a).

The RFB constitutes a very complex orogenic zone composed of several geological units, commonly separated by deep dextral shears, being the studied São Fidelis – Santo António de Pádua (SFSAP) sector located inside the Além Paraíba – Santo António de Pádua Shear (APPS) system (Fig. 2b). This megashear system deformed the area rocks imposing a NE trending transpressive shear deformation (FONSECA *et al*., 2008) associated with long-term HT/LP metamorphism (BENTO DOS SANTOS *et al*., 2008).

According to TROUW *et al*. (2000), the RFB can be divided in four major lithologic associations: a) reworked Archean to Paleoproterozoic basement rocks composed of metavolcanic-sedimentary sequences, granodioritic orthogneisses and intermediate granulites; b) a deformed meta-sedimentary sequence composed of pelitic schists and high grade migmatitic paragneisses with quartzite, calc-silicate and amphibolite intercalations; c) molasic sedimentary basins; and d) widespread granitoid intrusive bodies with different tectonic settings, from pre- to post-collision stages of the Brasiliano orogenic system (CAMPOS NETO & FIGUEIREDO, 1995; TROUW *et. al*., 2000; PEDROSA SOARES & WIEDMANN-LEONARDOS, 2000).

HEILBRON & MACHADO (2003) and VALLADARES *et al*. (2008) divided the central RFB into four tectonic/lithologic/geochronological domains as *klippen* thrusted against the São Francisco Craton. According to these authors, the central sector of RFB includes from NW to SE: a) the Occidental Domain, a pre-1.8 Ga passive margin succession, considered to be the reworked margin of the São Francisco Craton (basement rocks); b) the Paraíba do Sul *klippe*, composed of amphibolite facies orthogneisses and meta-sediments; c) the Oriental

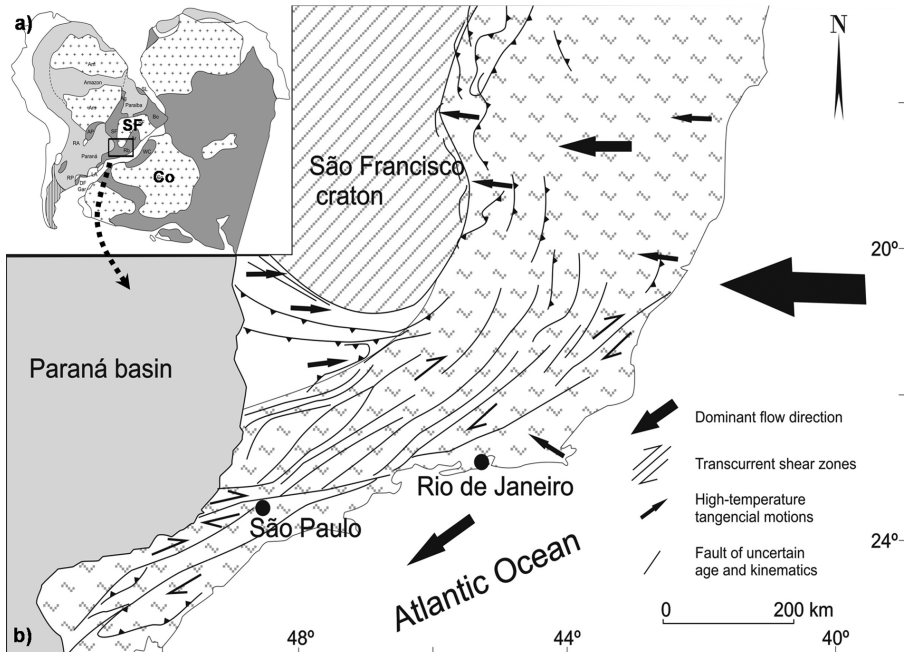

Fig. 2 – a) Central Ribeira Fold Belt (square) in the Western Gondwana amalgamation context (modified from TROUW *et al*., 2000). SF: São Francisco Craton; Co: Congo Craton; further abbreviations as in TROUW *et al.* (2000); b) Main regional structures from Central Ribeira Fold Belt and the Além Paraíba – Pádua Shear system (Modified from VAUCHEZ *et al.*, 1994).

Domain, comprising the Rio Negro Magmatic arc (Tupinambá, 1999) and fore-arc and back-arc meta-sedimentary sequences; and d) the Cabo Frio Terrane (Schmitt *et al*., 2008), an allochthonous terrane belonging to the West Congo Craton.

Regarding the RFB tectonic evolution, a dominant ensialic evolution with important crustal reworking has been favoured (Cordani *et al*., 1973), although subordinated oceanic crust subduction (and obduction) and continental accretion have also been considered (Pedrosa Soares & Wiedmann-Leonardos, 2000; Pedrosa Soares *et al*., 2001). Within the central part of the belt, in the Rio de Janeiro state, Heilbron *et al*. (1993) and Machado *et al*. (1996) proposed that the tectonometamorphic evolution of the Brasiliano Orogeny should be divided in: a) collision period (590 – 563 Ma) in which occurred the main deformation phases and metamorphism, with reworking and partial melting of older continental basement rocks and emplacement of several granitoid bodies; b) post-collision period at 535 – 520 Ma, corresponding to major dextral shear zones and retrograde metamorphism; c) post-tectonic period of orogenic collapse with emplacement of late granitic plutons at 490 Ma ago (Bento dos Santos *et al*., 2007).

The studied area, the SFSAP sector, is located in the central-north part of the RFB in northern Rio de Janeiro State (SE Brazil) and SE to the APPS main shear (near Santo António de Pádua) (Fig. 2 and 3). The SFSAP sector underwent complex polyphase ductile deformation, with thrusting dominantly to ESE, followed by NNE-SSW sub-horizontal dextral shearing that produced the elongated mineral fabric observed in the studied rocks (Bascou *et al*., 2002; Fonseca *et al*., 2008). In the studied area three main deformation phases can be observed. As outlined by Fonseca *et al*. (2008), the earliest deformation event (D_1) corresponds to high temperature (ductile) thrusts (250°, 55-70° NW), that were mostly erased by the main syn- to post-metamorphic peak D_2 event. This corresponds to the dextral megashear APPS system (50-65°, 70-85° NW). Finally, a D_3 fragile/brittle event is simultaneous with reactivation of D_2 conjugated fault systems (290-320°, subvertical).

Intense granulite facies metamorphism produced generalized migmatization and granitoid production by partial melting of paragneisses. Outcrops in the area comprise the referred migmatites, granulites and blastomylonites that resulted from late retrogression of the other rock types. Migmatites (Fig. 4a-b) show a clear

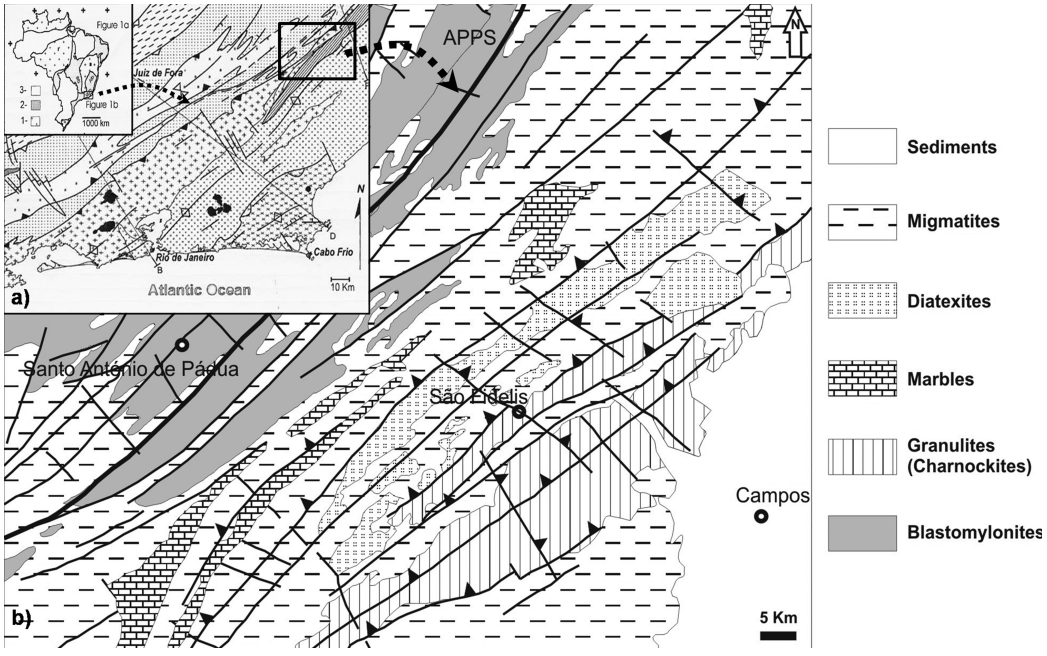

Fig. 3 – a) Location of the studied São Fidelis – Santo António de Pádua sector in central Ribeira Fold Belt, northern Rio de Janeiro State, SE Brazil (Modified from Trouw *et al.*, 2000; Heilbron & Machado, 2003). Lithologic domains are presented as in Heilbron & Machado, 2003; b) Simplified geological map of the São Fidelis – Santo António de Pádua sector showing the main lithologic units and structures present.

separation of gneissic paleosome and aplitic or pegmatitic neosome (Migmatite terminology as recommended by WIMMENAUER & BRYHNI, 2007). These rocks present gneissic foliation and banding, as well as clear evidences of late deformation and retrogression. These are associated with large elongated or rounded, undeformed and homogeneous granitic to migmatitic batholiths (diatexites), that represent a more advanced stage of anatexis of the migmatites. Marbles are occasionally interlayered in the migmatites as decametric to kilometric thick bands or small metric pockets. In the study area, granulites range from charnockites (s. s.) (Fig. 4c) to enderbites (basic granulites) that crop out as elongated NE-SW trending massifs and are overthrusted onto the migmatites during D_2 and D_3 deformation phases (FONSECA *et al*., 2008).

Blastomylonites resulted from the deformation and retrogression of the other rock types in areas closer to the APPS main shears (Fig. 4d). They represent the deformed and retrogressed equivalents of the granulites (mainly) and of the migmatites.

3. PETROGRAPHY

Petrographic observations and a mineral chemistry synthesis for the studied rocks are provided in this section with the exception of garnet and biotite mineral chemistry that will be provided with more detail below.

3.1. Migmatites

Paleosome commonly comprises a g + bi + q + pl (X_{an} = 0.26 – 0.43; X_{or} = 0.01 – 0.04) + ksp (X_{ab} < 0.1; X_{an} < 0.01) ± mt ± sill ± ilm (Mineral abbreviations according to POWELL & HOLLAND, 1999) gneissic association, whereas the neosomatic fraction consists of a g + bi + pl (X_{an} = 0.27 – 0.42; X_{or} = 0.01 – 0.04) + q + ksp (X_{ab} < 0.1; X_{an} < 0.01) ± sill ± ap mineral association (Fig. 5a). Migmatites do not show significant compositional difference between paleosome and neosome, including for garnets and biotites (see below). The

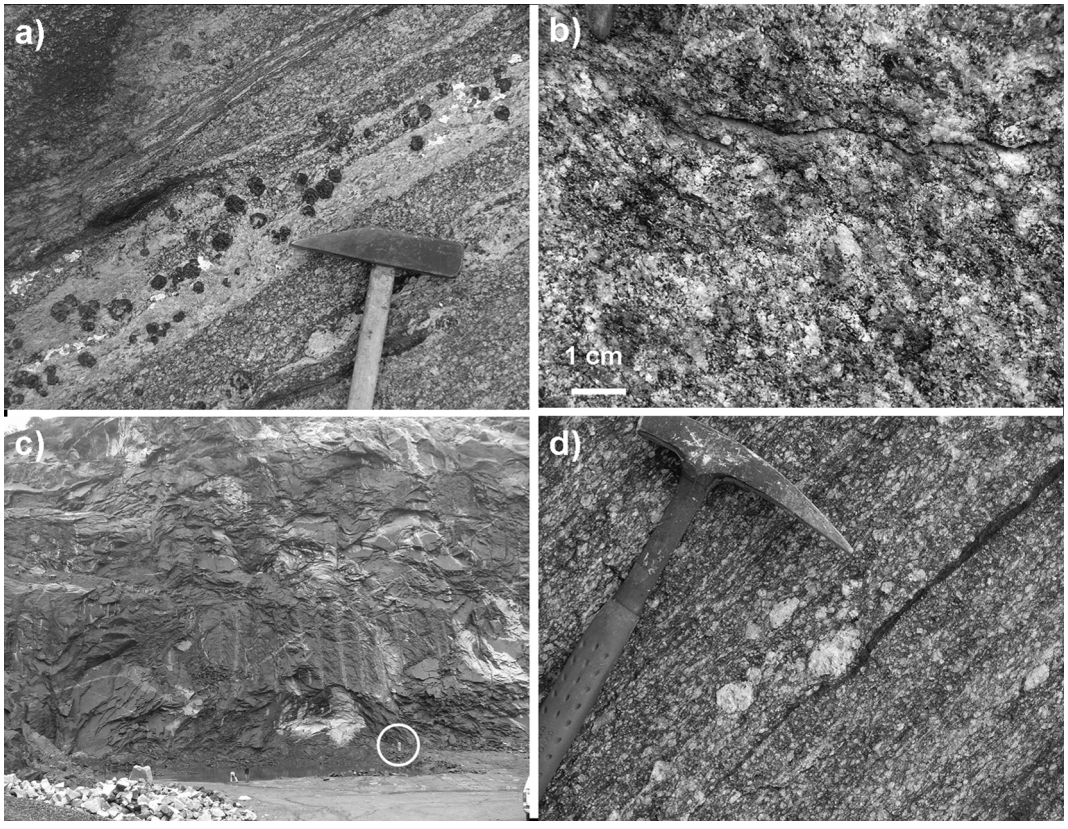

Fig. 4 – a) Garnet migmatites with clear separation of gneissic paleosome and aplitic neosome. b) Homogeneous undeformed migmatites with granitic/diatexitic aspect. c) Elongated granulite massif (circle evidences a person for scale purposes). d) Blastomylonitic occurrence with plagioclase neoblasts.

granolepidoblastic texture present in both paleosome and neosome, largely defined by the biotite + quartz association, is commonly obliterated by coarse grained, sometimes centimetric, subhedral or rounded poikiloblastic garnet, plagioclase and K-feldspar granoblasts. They frequently have matrix mineral inclusions, such as biotite, quartz and magnetite. These megablasts are usually deformed, bent or cracked and show recrystallized rims. The garnet – plagioclase – K-feldspar granoblastic assemblage represents the metamorphic peak paragenesis of the migmatites, possibly with small amounts of quartz and residual biotite.

The presence of biotite and sillimanite at garnet rims is a clear evidence of retrogression by garnet consumption. Symplectitic biotite + quartz + sillimanite growth after garnet is a common feature of these rocks. In some cases, these migmatites are intensively sheared, originating a fine grained mylonitic banding with abundant sillimanite (Fig. 5b).

3.2. Granulites

Isotropic charnockites (s. s.) show a medium to coarse sized granoblastic texture with megablastic (sometimes centimetric) subhedral g + pl (X_{an} = 0.29 – 0.51; X_{or} = = 0 – 0.03) + ksp (X_{ab} < 0.1 and X_{an} < 0.01) + opx (X_{en} = 0.39 – 0.48; X_{wo} < 0.03) assemblage. Bi + q + mt + ilm + ap + zrc are only present as diffuse, rarely orientated, matrix minerals (Fig. 5c). Biotites are frequently included in garnet and rarely in orthopyroxene megablasts. Bi + q symplectites are common around garnet and pyroxene rims, revealing that the retrometamorphic path involved significant deformation with decompression.

Some granulites are extensively sheared and retrogressed, showing a fine grained mylonitic or cataclastic texture with g + bi + pl + q + ksp + opx (relic) ± ap ± hb (X_{Mg} = 0.35 – 0.65) mineral assemblage (Fig. 5d). Metamorphic peak minerals (pl + ksp + q + opx + g) are intensively deformed, fractured, grinded and replaced by an amphibolite facies assemblage of bi + hb.

Enderbites are banded, medium to coarse grained and have a subhedral g + pl (X_{an} = 0.29 – 0.51; X_{or} = = 0 – 0.03) + opx (X_{en} = 0.41 – 0.44; X_{wo} < 0.02) + cpx (X_{en} = 0.30 – 0.35; X_{wo} = 0.42 – 0.48) metamorphic peak paragenesis. This assemblage is often replaced by the hb (X_{Mg} = 0.35 – 0.65) + pl (X_{an} = 0.29 – 42; X_{or} = 0 – 0.03) ± bi amphibolite facies assemblage (Fig. 5e).

3.3. Blastomylonites

Migmatites and granulites are profusely deformed and retrogressed in the near region of Santo António de Pádua, centre of the APPS system. There, it is very difficult to determine if the observed rocks were granulites or migmatites because of the blastomylonitic transformation they experienced. Therefore, the broad term blastomylonite is employed.

Petrographic features indicate that they are equivalent to their undeformed counterparts, with the exception of having a profuse equigranular mylonitic texture and finely recrystallized mineral grains (Fig. 5f). Mineralogical replacement of metamorphic peak assemblage progresses in the same way as previously stated for migmatites and granulites, but in blastomylonites there are only remnants of the high grade paragenesis. Therefore, the typical mineral assemblage of blastomylonites is pl (X_{an} = 0.17 – 0.55; X_{or} = 0.01 – 0.02) + bi + q + ksp (X_{ab} < 0.22; X_{an} < 0.01) with some small relics of the high temperature minerals, such as garnet, orthopyroxene (X_{en} = 0.41 – 0.44; X_{wo} < 0.02) or clinopyroxene (X_{en} = 0.30 – 0.35; X_{wo} = 0.42 – 0.48).

4. GARNET AND BIOTITE MINERAL CHEMISTRY

Samples were prepared for the different types of analyses at the Instituto de Geociências da Universidade de São Paulo (IGc-USP) and at the Departamento de Geologia da Faculdade de Ciências da Universidade de Lisboa (DG-FCUL).

Mineral composition data were determined on carbon coated polished thin sections using a JEOL JXA 733 wavelength dispersive Electron Microprobe, at the Centro de Geologia da Faculdade de Ciências da Universidade de Lisboa (CeGUL). Minerals were analysed with an acceleration voltage of 15 kV and a current of 25 nA, using a beam of 5 μm. Both natural and synthetic silicates were used as standards. Errors are typically below 1.5 wt% for major elements.

An extensive mineral chemistry study on garnets, biotite inclusions in garnets and matrix biotites was performed in the studied rocks, namely major element analyses of rim – core – rim (RCR) profiles in garnets and garnet – biotite interface (GBI) profiles in garnets. These results were obtained in granulites and in the paleosomes (mainly) of migmatites. However, no significant

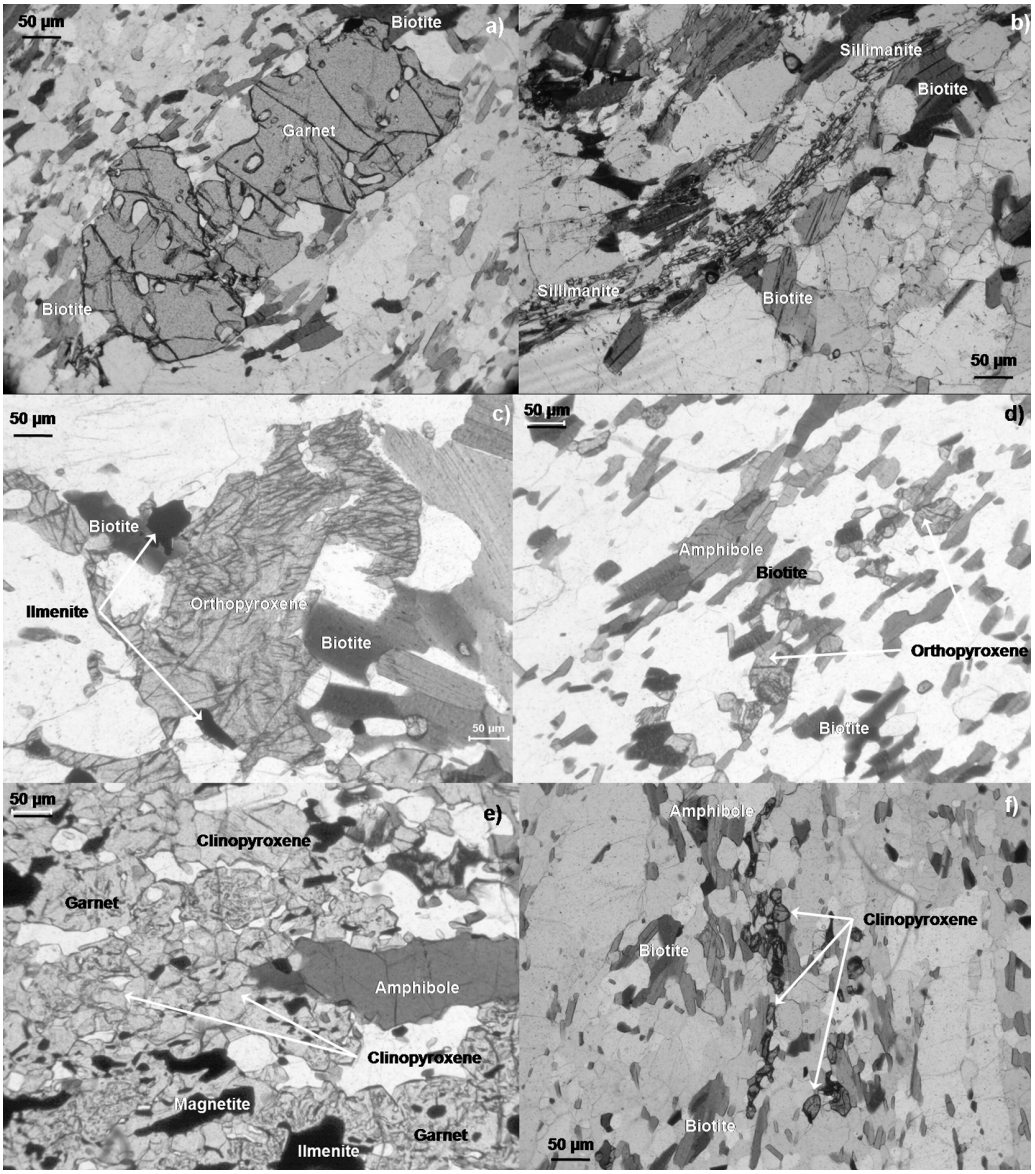

Fig. 5 – Petrographic observations of the studied rocks: a) Migmatite paleosome with a garnet megablast surrounded by a granolepidoblastic matrix. b) Deformed and sheared migmatite neosome with retrogressed biotite + quartz + sillimanite assemblage. c) Isotropic granulites showing an orthopyroxene megablast surrounded by late biotite. d) Deformed and sheared granulites showing fine grained mylonitic granolepidoblastic texture. e) Coarse grained enderbite with some amphibolitization of the peak garnet + clinopyroxene assemblage. f) Profuse equigranular mylonitic texture with abundant finely recrystallized mineral grains in blastomylonites.

compositional variation was found for paleosomes and neosomes of the migmatite samples.

The following mineral chemistry data on garnets and biotites is summarized due to the extensive number of chemical analyses performed in both garnet and biotite (over 2500 and over 1800 analyses, respectively). Examples of RCR profiles of the studied garnets are provided in Fig. 6 as a synthesis. GBI profiles in garnets and summarized analyses of biotite inclusions are provided in the petrological cooling rates section.

Mineral chemistry results for blastomylonites are presented as a synthesis in order to be compared with their undeformed equivalents. However, due to the extensive shearing and metamorphic recrystallization that characterize these rocks, no attempt to obtain petrological cooling rates in blastomylonites was performed.

4.1. Garnets

Garnets are almandine-rich in all rock types, with X_{alm} always higher than 0.54 and always with Mg-richer cores compared to the rims. All rock types show the same zoning pattern from core (Mg-richer) to rim (Fe-richer), but display very different range of values, namely X_{alm} = 0.61 to 0.75 and X_{py} = 0.07 to 0.21 for granulites, X_{alm} = 0.54 to 0.77 and X_{py} = 0.07 to 0.37 for migmatites and X_{alm} = 0.59 to 0.77 and X_{py} = 0.11 to 0.19 for blastomylonites. Migmatites do not show significant compositional difference between paleosome and neosome. They present the highest pyrope contents and variable grossular contents ranging from X_{gr} = 0.01 to 0.27. Although the highest value of X_{gr} is present in a migmatite, granulites are normally richer in calcium, with X_{gr} ranging from 0.02 to 0.22. Spessartine contents are always low (normally $X_{spss} < 0.1$), reaching a maximum of 0.13 in granulites and migmatites. Examples of compositional RCR profiles of garnets from both rock types are provided in Fig. 6a-d.

4.2. Biotites

Granulites have matrix biotites with X_{Mg} ranging from 0.39 to 0.55 and high TiO_2 contents ranging from 3.8 to 6.3 wt%. Migmatites show a great range of X_{Mg} contents ranging from 0.36 to Fe-poor matrix biotites with X_{Mg} = 0.76, whereas TiO_2 contents range between 3.7 to 4.5 wt%. This X_{Mg} range is observable in both paleosome and neosome. Blastomylonites show X_{Mg} values similar to granulites (0.39 to 0.55) and TiO_2 contents ranging from 4.9 – 5.8 wt%. Fe/Mg composition and size of biotite inclusions in garnet from migmatites and granulites are synthesized in Tables 1a-f and will be further discussed below.

5. PETROLOGICAL COOLING RATES

As previously referred, diffusion induced by compositional variation in the garnet-biotite interface is a function of $Kd_{(Mg/Fe)Garnet\text{-}Biotite}$ in response to thermal changes, such as cooling during retrograde path. Fe/(Fe+Mg) results in garnet and biotite inclusions can thus be transformed in its respective closure temperature (T_c) and converted in terms of thermochronological evolution by obtaining cooling rates.

This work uses two significantly different methodologies that relies on Fe-Mg exchange between garnet and biotite inclusions: a) the method proposed by Spear & Parrish (1996), based on Fe-Mg exchange modelling between a garnet megablast and its corresponding biotite inclusions; b) the method proposed by Gangully *et al*. (1998) that uses garnet compositional profiles near the garnet/biotite inclusion interface in order to infer metamorphic cooling rates. These methods are relatively recent but have been applied successfully in other orogenic belts (e.g.: Spear & Parrish, 1996; Munhá *et al*., 2005; Storm & Spear, 2005).

5.1. The Spear & Parrish (1996) method

This method is based on Fe-Mg exchange modelling between a garnet megablast and its corresponding biotite inclusions. Fe/(Fe+Mg) variations will be a function of biotite inclusions size if diffusion is exclusive between garnet and the several biotites included. This will produce larger compositional variations in smaller biotite inclusions. Therefore, Fe/(Fe+Mg) in each inclusion can be transformed in its respective apparent closure temperature using the garnet's core composition and the Ferry & Spear (1978) thermometer (Tab. 1a-f). Cooling rates are obtained using the diffusion coefficients of Chakraborty & Gangully (1992), as shown in Fig. 7 and 8.

Fig. 7 shows that some Fe/Mg results are indeed correlated with biotite inclusions size, providing trends for some migmatites and granulites, whereas others provide significant dispersion and no correlation. However, samples that provide correlation trends between Fe/Mg results and biotite inclusions size are not significantly different in Fe/Mg contents, having Fe/Mg variation < 0.2, in most cases (Table 1a-f). This is problematic, since small amplitudes in Fe/Mg of biotite inclusions provide a very narrow variation for apparent closure temperatures, as can be seen in Table 1 and Fig. 8.

The several petrological cooling rates plots, summarized in Fig. 8, allow us to state that samples that show high Fe/Mg dispersion, also show significant closure temperature dispersion (Fig. 8 a-c) with cooling rates spanning from 0.1 to 200°C/Ma, whereas samples that show very narrow Fe/Mg variation provide flat closure temperature patterns (Fig. 8 d-f) with cooling rates spanning from 1 to 200°C/Ma.

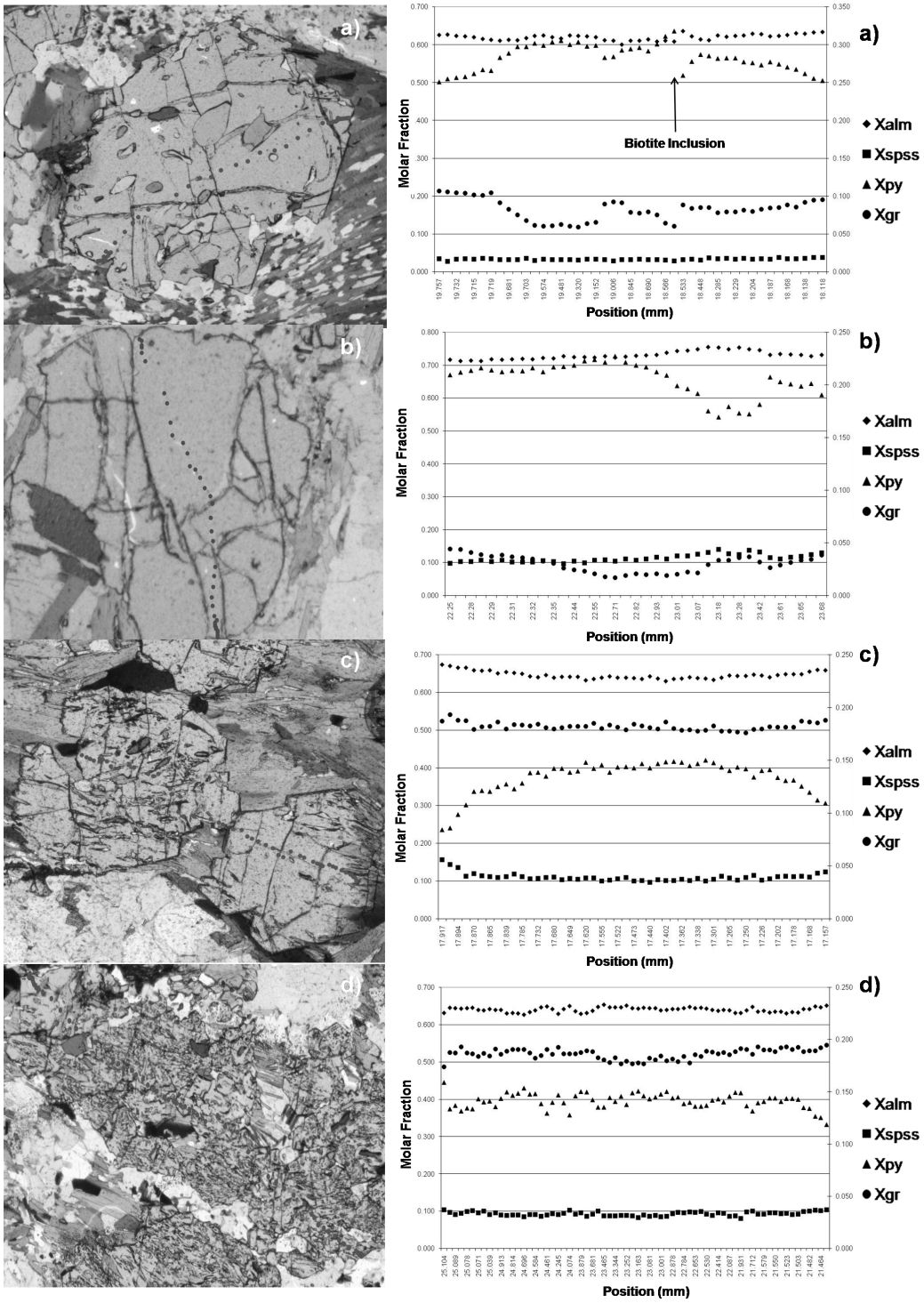

Fig. 6 – Examples of compositional RCR profiles in garnets from migmatites (Fig. 6a-b) and granulites (Fig. 6c-d). X_{alm} is always plotted in the main axis (at the left), whereas X_{spss}, X_{py} and X_{gr} are plotted in the secondary axis (at the right). Fig. 6a shows a typical zoning pattern for garnet (as described in the text), increasing substantially the Fe/(Fe+Mg) values in the core area due to the proximity of a biotite inclusion; Fig. 6b shows a rare RCR profile where garnet does not present the expect results, which is probably due to garnet consumption or some other heterogeneity; Fig. 6c shows a typical diffusive RCR profile for garnet with a zoning pattern where Fe and Mn decreases and Mg increases from rim to core; Fig. 6d shows the same zoning pattern, but only in one rim.

TABLE 1a

Garnet and respective biotite inclusions composition of migmatite 341a used for the application of the Spear & Parrish (1996) method. Also present is the dimension of each biotite inclusion and garnet's core composition. The latter was used together with each biotite Fe/Mg value to obtain each apparent closure temperature using the Ferry & Spear (1978) geothermometer.

Migmatite 341a						
Analysis	Dimension (μm)	Log Dimension	Fe^{2+}	Mg	Fe/Mg	T (ºC)
Biotite 4	40	1.60	2.851	1.982	1.438	637
Biotite 5	80	1.90	2.784	1.948	1.429	635
Biotite 7	30	1.48	2.853	1.949	1.464	644
Biotite 8	150	2.18	2.932	1.923	1.525	660
Biotite 46	70	1.85	2.888	1.946	1.484	650
Biotite 47	60	1.78	2.877	1.922	1.497	653
Biotite 48	30	1.48	2.892	1.99	1.453	641
Biotite 49	80	1.90	2.849	1.987	1.434	636
Biotite 50	150	2.18	2.906	1.914	1.518	658
Biotite 51	20	1.30	2.835	1.994	1.422	633
Biotite 52	70	1.85	2.875	1.961	1.466	645
Biotite 53	80	1.90	2.885	1.973	1.462	644
Garnet 1-3	X_{Alm}	X_{Spss}	X_{Py}	X_{Gr}		
	0.573	0.078	0.082	0.268		

TABLE 1b

Garnet and respective biotite inclusions composition of migmatite 13a used for the application of the Spear & Parrish (1996) method. Also present is the dimension of each biotite inclusion and garnet's core composition. The latter was used together with each biotite Fe/Mg value to obtain each apparent closure temperature using the Ferry & Spear (1978) geothermometer.

Migmatite 13a						
Analysis	Dimension (μm)	Log Dimension	Fe^{2+}	Mg	Fe/Mg	T (ºC)
Biotite 7	90	1.95	1.576	2.908	0.542	708
Biotite 9	200	2.30	1.345	3.336	0.403	589
Biotite 11	250	2.40	1.436	3.01	0.477	653
Biotite 13	230	2.36	1.286	3.411	0.377	565
Biotite 15	100	2.00	1.449	3.016	0.480	656
Biotite 17	60	1.78	1.484	3.012	0.493	666
Biotite 19	170	2.23	1.584	2.908	0.545	711
Biotite 21	100	2.00	1.384	3.184	0.435	616
Biotite 23	110	2.04	1.59	2.792	0.569	732
Biotite 25	170	2.23	1.376	3.013	0.457	635
Biotite 27	150	2.18	1.393	2.945	0.473	649
Biotite 29	200	2.30	1.501	3.027	0.496	669
Biotite 31	130	2.11	1.351	3.095	0.437	618
Garnet 2-4	X_{Alm}	X_{Spss}	X_{Py}	X_{Gr}		
	0.658	0.017	0.289	0.035		

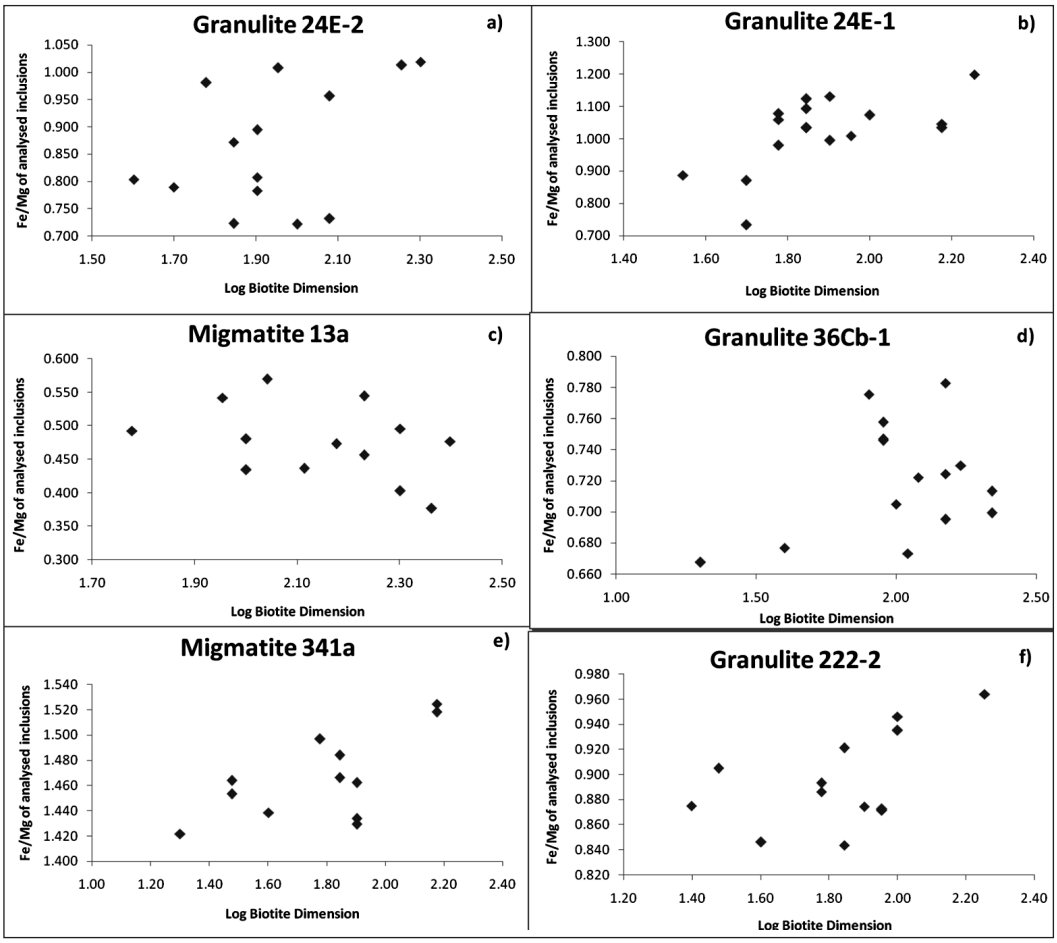

Fig. 7 – Examples of analysed biotite inclusions Fe/Mg results correlated with respective inclusions size for migmatites (Fig. 7c; 7e) and granulites (Fig. 7a; 7b; 7d; 7f). It is possible to observe that some present very high dispersion of results whereas some show a good correlation between Fe/Mg and biotite dimension.

.

TABLE 1c

Garnet and respective biotite inclusions composition of granulite 24E-1 used for the application of the SPEAR & PARRISH (1996) method. Also present is the dimension of each biotite inclusion and garnet's core composition. The latter was used together with each biotite Fe/Mg value to obtain each apparent closure temperature using the FERRY & SPEAR (1978) geothermometer.

Granulite 24E-1						
Analysis	Dimension (μm)	Log Dimension	Fe^{2+}	Mg	Fe/Mg	T (ºC)
Biotite 5	70	1.85	2.591	2.371	1.093	703
Biotite 7	60	1.78	2.604	2.416	1.078	697
Biotite 9	70	1.85	2.627	2.337	1.124	715
Biotite 11	50	1.70	2.278	2.616	0.871	612
Biotite 13	35	1.54	2.3	2.592	0.887	619
Biotite 21	70	1.85	2.555	2.471	1.034	679
Biotite 23	50	1.70	2.08	2.833	0.734	554
Biotite 54	70	1.85	2.418	2.337	1.035	679
Biotite 55	60	1.78	2.342	2.389	0.980	657
Biotite 56	90	1.95	2.316	2.294	1.010	669
Biotite 57	100	2.00	2.414	2.25	1.073	695
Biotite 58	60	1.78	2.444	2.307	1.059	689
Biotite 59	180	2.26	2.516	2.099	1.199	745
Biotite 60	150	2.18	2.45	2.342	1.046	684
Biotite 61	150	2.18	2.441	2.361	1.034	679
Biotite 62	80	1.90	2.533	2.239	1.131	718
Biotite 63	80	1.90	2.42	2.433	0.995	663
Garnet 1-3	X_{Alm}	X_{Spss}	X_{Py}	X_{Gr}		
	0.717	0.036	0.177	0.069		

TABLE 1d

Garnet and respective biotite inclusions composition of granulite 24E-2 used for the application of the SPEAR & PARRISH (1996) method. Also present is the dimension of each biotite inclusion and garnet's core composition. The latter was used together with each biotite Fe/Mg value to obtain each apparent closure temperature using the FERRY & SPEAR (1978) geothermometer.

Granulite 24E-2						
Analysis	Dimension (μm)	Log Dimension	Fe^{2+}	Mg	Fe/Mg	T (ºC)
Biotite 27	80	1.90	2.137	2.729	0.783	605
Biotite 29	40	1.60	2.193	2.73	0.803	614
Biotite 33	100	2.00	2.047	2.836	0.722	577
Biotite 64	120	2.08	2.334	2.44	0.957	682
Biotite 65	180	2.26	2.376	2.345	1.013	708
Biotite 66	70	1.85	1.987	2.748	0.723	578
Biotite 67	120	2.08	1.984	2.712	0.732	581
Biotite 68	80	1.90	2.108	2.611	0.807	616
Biotite 70	70	1.85	2.125	2.437	0.872	645
Biotite 72	50	1.70	2.091	2.65	0.789	608
Biotite 73	80	1.90	2.192	2.451	0.894	655
Biotite 74	90	1.95	2.38	2.361	1.008	706
Biotite 75	200	2.30	2.407	2.362	1.019	711
Biotite 76	60	1.78	2.323	2.369	0.981	693
Garnet 18-20	X_{Alm}	X_{Spss}	X_{Py}	X_{Gr}		
	0.713	0.037	0.186	0.065		

TABLE 1e

Garnet and respective biotite inclusions composition of granulite 36Cb-1 used for the application of the SPEAR & PARRISH (1996) method. Also present is the dimension of each biotite inclusion and garnet's core composition. The latter was used together with each biotite Fe/Mg value to obtain each apparent closure temperature using the FERRY & SPEAR (1978) geothermometer.

Granulite 36Cb-1						
Analysis	Dimension (μm)	Log Dimension	Fe^{2+}	Mg	Fe/Mg	T (ºC)
Biotite 6	110	2.04	1.949	2.895	0.673	642
Biotite 7	20	1.30	1.902	2.849	0.668	639
Biotite 8	150	2.18	2.014	2.78	0.724	671
Biotite 9	100	2.00	1.98	2.809	0.705	660
Biotite 10	90	1.95	2.056	2.714	0.758	690
Biotite 11	150	2.18	1.98	2.848	0.695	655
Biotite 12	220	2.34	1.979	2.83	0.699	657
Biotite 13	90	1.95	2.048	2.742	0.747	684
Biotite 81	150	2.18	2.032	2.596	0.783	704
Biotite 82	90	1.95	2.051	2.75	0.746	683
Biotite 83	170	2.23	1.966	2.694	0.730	674
Biotite 84	120	2.08	2.012	2.786	0.722	670
Biotite 85	220	2.34	1.99	2.79	0.713	665
Biotite 86	40	1.60	1.939	2.865	0.677	644
Biotite 87	80	1.90	2.08	2.682	0.776	700
Garnet 1-5	X_{Alm}	X_{Spss}	X_{Py}	X_{Gr}		
	0.679	0.027	0.208	0.086		

TABLE 1f

Garnet and respective biotite inclusions composition of granulite 222-2 used for the application of the SPEAR & PARRISH (1996) method. Also present is the dimension of each biotite inclusion and garnet's core composition. The latter was used together with each biotite Fe/Mg value to obtain each apparent closure temperature using the FERRY & SPEAR (1978) geothermometer.

Granulite 222-2						
Analysis	Dimension (μm)	Log Dimension	Fe^{2+}	Mg	Fe/Mg	T (ºC)
Biotite 29	100	2.00	2.339	2.501	0.935	647
Biotite 30	60	1.78	2.342	2.622	0.893	629
Biotite 31	25	1.40	2.204	2.519	0.875	622
Biotite 32	70	1.85	2.243	2.659	0.844	608
Biotite 33	180	2.26	2.384	2.473	0.964	659
Biotite 34	80	1.90	2.209	2.526	0.875	621
Biotite 35	30	1.48	2.256	2.493	0.905	634
Biotite 36	40	1.60	2.264	2.676	0.846	609
Biotite 84	60	1.78	2.295	2.590	0.886	626
Biotite 86	100	2.00	2.296	2.427	0.946	651
Biotite 87	70	1.85	2.368	2.571	0.921	641
Biotite 88	90	1.95	2.317	2.659	0.871	620
Biotite 89	90	1.95	2.312	2.650	0.872	621
Garnet 27-28	X_{Alm}	X_{Spss}	X_{Py}	X_{Gr}		
	0.624	0.028	0.149	0.199		

5.2. The GANGULLY *et al.* (1998) method

Another attempt to obtain petrologic cooling rates with compositional Fe-Mg diffusion between garnet and biotite was performed by using the GANGULLY *et al.* (1998) method. It consists in modelling the variation of garnet's composition in the interface with a biotite inclusion, from the biotite/garnet interface to an area of the garnet that is far enough from the compositional effect caused by the biotite inclusion, i.e. the *plateau* composi-

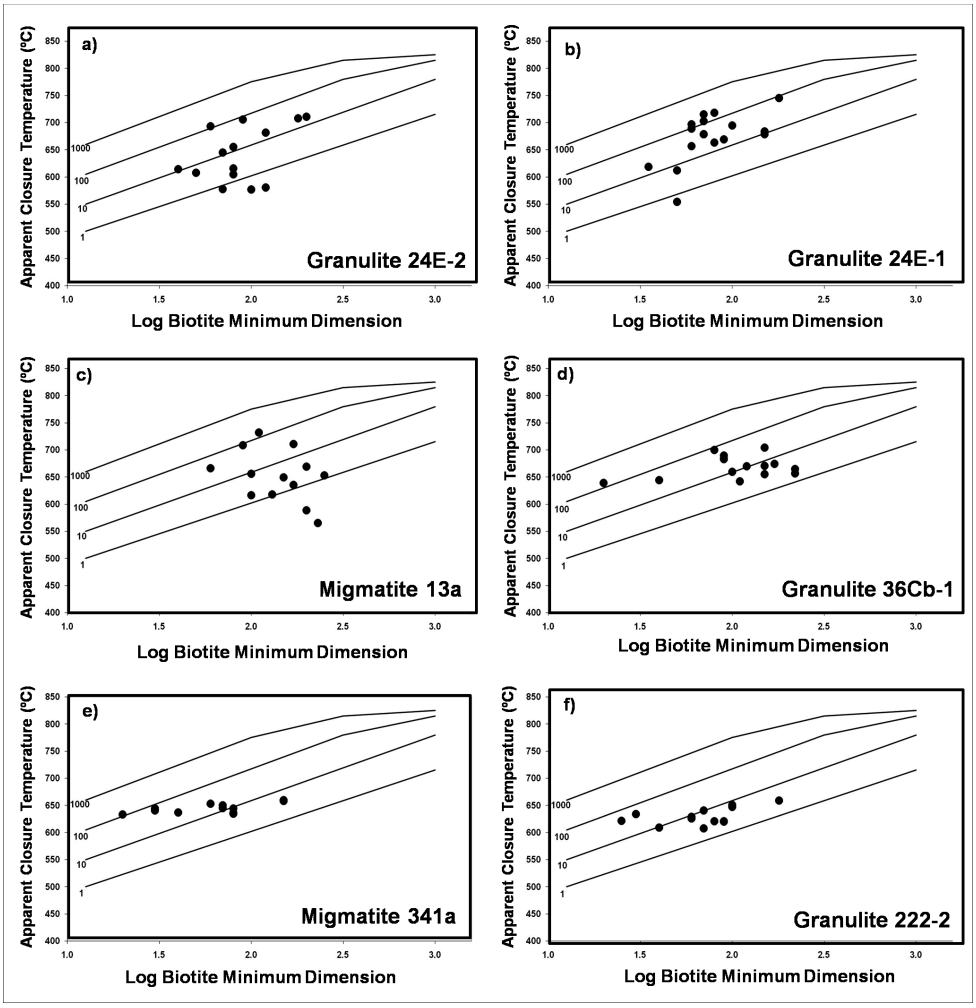

Fig. 8 – Examples of petrological cooling rates for the studied migmatites (Fig. 8c; 8e) and granulites (Fig. 8a; 8b; 8d; 8f). Samples are displayed in the same order as in Fig. 7. Some samples show a great dispersion of results, making it impossible to accurately depict any trend for cooling rates (Fig. 8a-c), whereas others show a very narrow closure temperature variation (Fig. 8d-f), suggesting homogenized Fe/Mg values. Apparent closure temperatures vs. biotite dimensions are plotted with the Chakraborty & Gangully (1992) diffusion coefficients. Cooling rates are presented in ºC/Ma.

tion of garnet. This method is significantly opposed to the previous one because it does not use the compositional variation of biotite inclusions, but the compositional variation of garnet around the biotite inclusion. For this second method we used the software "GARBIDIF" developed by MUNHÁ (personal communication) and the garnet Fe-Mg diffusion parameters of Gangully *et al*. (1998).

A GBI compositional profile was obtained for granulite 153c and migmatite 73A (Tab. 2 a-b; Fig. 9-10) around the respective biotite inclusions. However, the granulite garnet shows no Fe/(Fe/Mg) zoning in the interface with the biotite inclusion, even with a minimum distance of analyse to the garnet – biotite interface being 5 μm (Fig. 9). Migmatite 73A GBI profile shows 220 μm size Fe/(Fe/Mg) zoning in the interface with the biotite inclusion (Fig. 10). This will be discussed in the following section.

6. DISCUSSION

The results obtained with the Spear & Parrish (1996) method are very difficult to interpret both for granulites and migmatites, because biotite dimension (logarithmic) vs. garnet – biotite apparent closure

Fig. 9 – GBI compositional profile of garnet with no zoning pattern from near the biotite inclusion (at the left) to garnet core (at the right) in granulite 153c. Minimum analysed distance to interface is 5 µm. X_{alm} is plotted in the main axis (at the left), whereas X_{spss}, X_{py} and X_{gr} are plotted in the secondary axis (at the right).

TABLE 2a

GBI profile of granulite 153c used in the application of the GANGULLY *et al*. (1998) method. Also present is the distance of the analysed garnet to the garnet-biotite inclusion interface. Fe/(Fe/Mg) variation is reduced, spanning from 0.825 to 0.808, suggesting that no Fe/(Fe/Mg) diffusion occurred in the garnet – biotite interface.

Analysis	Distance (µm)	X_{Py}	X_{Alm}	X_{Spss}	X_{Gr}	Fe/(Fe+Mg)
Garnet 01	2	0.141	0.642	0.036	0.182	0.820
Garnet 02	5	0.144	0.639	0.035	0.182	0.816
Garnet 03	9	0.138	0.641	0.037	0.184	0.823
Garnet 04	14	0.139	0.646	0.035	0.181	0.823
Garnet 05	20	0.146	0.640	0.034	0.180	0.814
Garnet 06	24	0.143	0.640	0.038	0.179	0.818
Garnet 07	22	0.143	0.637	0.037	0.183	0.816
Garnet 08	33	0.144	0.639	0.035	0.182	0.816
Garnet 10	39	0.143	0.639	0.035	0.183	0.817
Garnet 11	43	0.145	0.634	0.037	0.184	0.814
Garnet 12	47	0.147	0.637	0.035	0.182	0.813
Garnet 13	42	0.147	0.631	0.037	0.185	0.811
Garnet 14	52	0.145	0.635	0.036	0.183	0.814
Garnet 15	56	0.145	0.640	0.035	0.181	0.816
Garnet 16	60	0.147	0.639	0.034	0.181	0.813
Garnet 17	54	0.137	0.643	0.037	0.184	0.825
Garnet 19	76	0.146	0.636	0.035	0.184	0.813
Garnet 20	71	0.146	0.636	0.035	0.183	0.813
Garnet 21	80	0.148	0.640	0.035	0.177	0.812
Garnet 22	80	0.151	0.634	0.036	0.179	0.808
Garnet 23	75	0.150	0.635	0.035	0.181	0.809
Garnet 24	79	0.146	0.631	0.037	0.185	0.812
Garnet 25	79	0.143	0.638	0.036	0.184	0.817
Garnet 26	88	0.151	0.630	0.036	0.182	0.806
Garnet 27	88	0.146	0.633	0.037	0.184	0.812
Garnet 28	88	0.147	0.633	0.038	0.182	0.812
Garnet 29	88	0.148	0.630	0.040	0.183	0.810
Garnet 30	88	0.150	0.632	0.037	0.181	0.808
Garnet 31	99	0.143	0.636	0.037	0.184	0.816
Garnet 32	102	0.143	0.640	0.036	0.181	0.817
Garnet 33	113	0.145	0.634	0.037	0.183	0.814
Garnet 34	113	0.147	0.631	0.039	0.183	0.812
Garnet 35	126	0.148	0.636	0.034	0.182	0.811
Garnet 36	133	0.146	0.637	0.034	0.184	0.814
Garnet 37	142	0.148	0.633	0.036	0.183	0.811
Garnet 38	150	0.147	0.634	0.035	0.183	0.812
Garnet 39	159	0.148	0.631	0.036	0.185	0.810
Garnet 40	171	0.148	0.642	0.034	0.175	0.813

TABLE 2b

GBI profile of migmatite 73A used in the application of the GANGULLY *et al*. (1998) method. Also present is the distance of the analysed garnet to the garnet-biotite inclusion interface. Fe/(Fe/Mg) variation is significant, spanning from 0.676 to 0.623, suggesting that Fe/(Fe/Mg) diffusion in the garnet – biotite interface occurred.

Analysis	Distance (µm)	X_{Py}	X_{Alm}	X_{Spss}	X_{Gr}	Fe/(Fe+Mg)
Garnet 01	5	0.311	0.650	0.013	0.026	0.676
Garnet 02	9	0.325	0.636	0.013	0.026	0.662
Garnet 03	19	0.335	0.627	0.013	0.025	0.652
Garnet 04	24	0.339	0.623	0.012	0.027	0.647
Garnet 05	32	0.344	0.617	0.013	0.026	0.642
Garnet 06	43	0.346	0.617	0.012	0.026	0.641
Garnet 07	35	0.341	0.621	0.011	0.027	0.646
Garnet 08	49	0.349	0.613	0.011	0.027	0.637
Garnet 09	66	0.352	0.611	0.011	0.026	0.634
Garnet 10	72	0.346	0.616	0.011	0.027	0.640
Garnet 11	80	0.348	0.615	0.011	0.026	0.639
Garnet 12	89	0.350	0.612	0.011	0.027	0.636
Garnet 13	96	0.346	0.618	0.010	0.026	0.641
Garnet 14	99	0.350	0.612	0.013	0.026	0.636
Garnet 15	107	0.351	0.612	0.012	0.026	0.636
Garnet 16	113	0.349	0.614	0.010	0.027	0.638
Garnet 17	116	0.350	0.612	0.012	0.026	0.633
Garnet 18	118	0.353	0.610	0.011	0.025	0.636
Garnet 19	127	0.354	0.606	0.013	0.027	0.632
Garnet 20	132	0.355	0.605	0.012	0.027	0.630
Garnet 21	136	0.356	0.606	0.012	0.026	0.630
Garnet 22	142	0.351	0.610	0.013	0.027	0.635
Garnet 23	145	0.356	0.606	0.011	0.027	0.630
Garnet 24	156	0.358	0.603	0.012	0.027	0.628
Garnet 25	161	0.357	0.605	0.012	0.026	0.629
Garnet 26	166	0.351	0.610	0.012	0.027	0.634
Garnet 27	172	0.359	0.602	0.013	0.027	0.627
Garnet 28	174	0.361	0.601	0.012	0.026	0.628
Garnet 29	177	0.354	0.608	0.011	0.026	0.624
Garnet 30	182	0.358	0.603	0.013	0.027	0.632
Garnet 31	192	0.360	0.602	0.011	0.026	0.625
Garnet 32	204	0.356	0.608	0.012	0.025	0.631
Garnet 33	231	0.361	0.601	0.011	0.027	0.625
Garnet 34	242	0.362	0.599	0.012	0.026	0.623
Garnet 35	255	0.360	0.602	0.012	0.027	0.626
Garnet 36	272	0.370	0.619	0.011	0.025	0.625
Garnet 37	293	0.368	0.620	0.012	0.025	0.627
Garnet 38	313	0.368	0.619	0.013	0.027	0.627
Garnet 39	336	0.367	0.621	0.012	0.026	0.629
Garnet 40	355	0.370	0.618	0.011	0.027	0.625

temperatures show very high dispersion of results. It is, therefore, impossible to discriminate a cooling rates trend (Fig. 8). Other samples (Fig. 8 d-f) show a very low range of apparent closure temperatures for biotites that are very different in terms of size. This suggests that garnet and its biotite inclusions must have been reequilibrated (re-homogenized) at high temperatures and then cooled very fast, inhibiting significant change in the Fe/Mg of biotite inclusions, and consequently, in the apparent temperatures. In both cases, important assumptions for the application of this method were not maintained: cationic exchange with mass balance preservation between garnet and biotite inclusions (i.e. close system behaviour) and/or sufficiently discriminating Fe/Mg variation in biotite inclusions correlated with respective size. Therefore, although this methodology provided some insights regarding the general trends for cooling patterns, it did not constrain accurately the cooling rates of the studied rocks.

The obtained compositional profiles using the Gangully *et al*. (1998) method also provided unsatisfactory results, since granulite 153c shows no type of Fe/(Fe/Mg) garnet zoning in the interface with the biotite inclusion (Fig. 9). This implies that garnet was equilibrated with a significant amount of biotite at high temperatures, followed by very fast cooling that did not allow the formation of any type of zoning pattern (minimum distance of the analyses to the garnet – biotite interface is 5 μm). This hampers any type of inference regarding petrological cooling rates. However, it is possible to conclude (qualitatively) that it must have been high temperature maintenance for a substantial amount of time (that allowed for the garnet to be homogenized), followed by a period of very fast cooling rates, as evidenced in samples 36Cb-1, 341a and 222-2 (Fig. 8 d-f). This is in overall agreement with geochronological cooling rates provided by Bento dos Santos *et al*. (2008) (see below).

Migmatite 73A garnet compositional profile (Fig. 10) in the interface with the biotite inclusion is significantly opposed to the previous one, because it presents a pronounced zoning pattern from Fe/(Fe+Mg) higher values close to the biotite to more Mg-rich values far from the interface with the biotite inclusion.

The profile is divided in three parts (as evidenced in Fig. 10): zone 1 (far from the biotite inclusion) shows plateau values (Fe/(Fe+Mg) = 0.623 – 0.629; average Fe/(Fe+Mg) = 0.6261), equivalent with the garnet's core composition far from the inclusions (compare with Fig. 11 that shows the RCR profile for the referred garnet; average core Fe/(Fe+Mg) = 0.628). This area of the profile is absent of Fe-Mg cation exchange between the garnet and the inclusion, i.e. there is preservation of garnet's initial composition; zone 2 shows an apparent arithmetic increase of Fe/(Fe + Mg) values according with proximity to the biotite inclusion; and, finally, zone 3 shows an exponential Fe/(Fe + Mg) increase with proximity to the biotite inclusion.

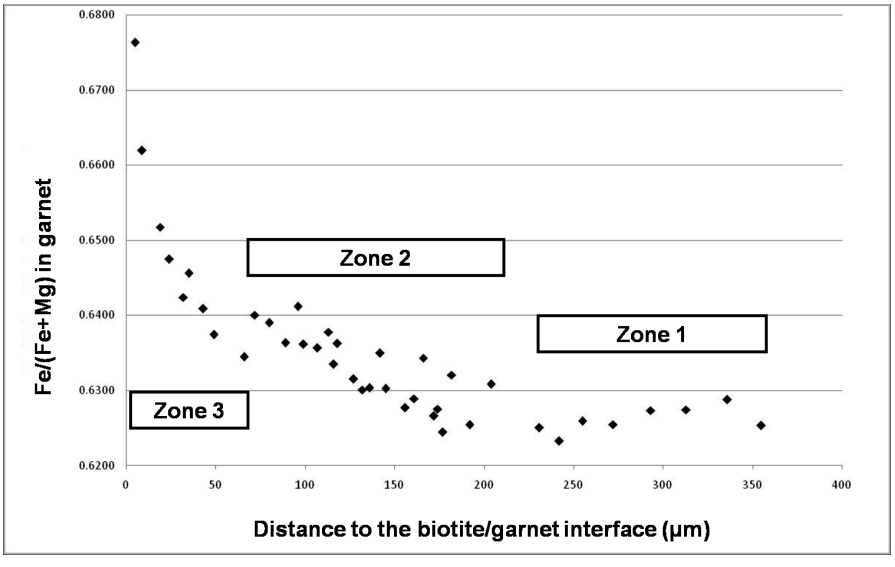

Fig. 10 – Zoned GBI compositional profile of the studied garnet in migmatite 73A, as explained in the text.

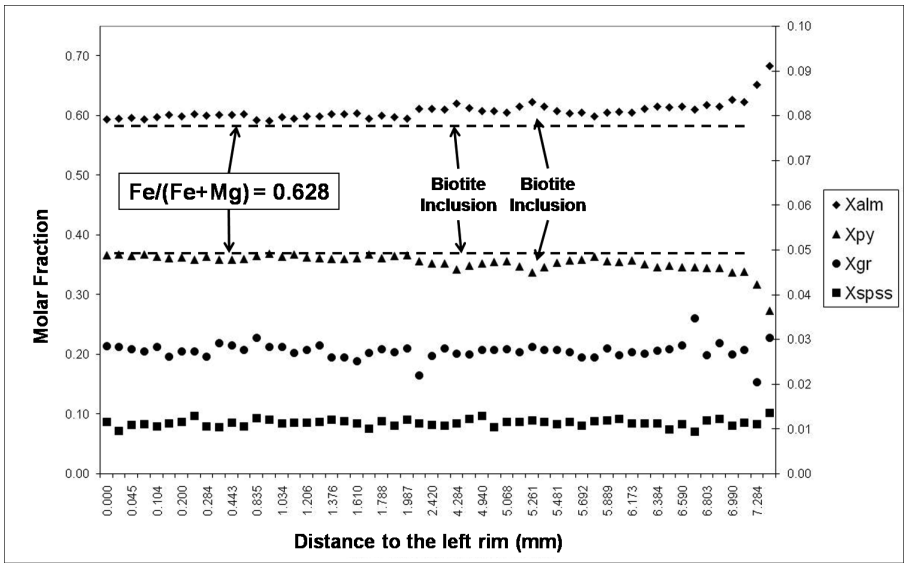

Fig. 11 – RCR compositional profile of the studied garnet in migmatite 73A. X_{alm} and X_{py} are plotted in the main axis (at the left), whereas X_{spss} and X_{gr} are plotted in the secondary axis (at the right). This garnet does not show a typical RCR zoning pattern, because the left rim shows plateau values, probably due to retrograde consumption of garnet.

Modelling for this compositional profile is based on the assumption that Fe-Mg cationic exchange between garnet and corresponding biotite inclusion is exclusive and that mass balance preservation between both minerals occurred. Therefore, the effective dimensions of each mineral were used (garnet radius (R_{Garnet}) is 1 mm and the average biotite dimension ($R_{Biotite}$) is 0.1 mm) at different cooling rates. The other diffusive parameters used were $D_{Fe/Mg}^{Biotite} = 100D_{Fe/Mg}^{Garnet}$; Initial Temperature ($T_i$) = 800°C and Initial Pressure (Pi) = 8 kbar (BENTO DOS SANTOS, 2008; MUNHÁ *et al*., 2008); $Fe/(Fe+Mg)_i^{Garnet} = 0.6261$).

After performing several modelling with different cooling rates from 5 to 200°C/Ma (Fig. 12), it became evident that it was impossible to adequately adjust any cooling rate pattern to the obtained compositional profile, especially in zone 2. The mentioned modelling, besides not adjusting adequately to the profile, apparently would imply the possibility of having cooling rates so disparate as 5 and 200°C/Ma (Fig. 12).

The fact that none of the obtained modelling is adjustable to the GBI profile and because zone 2 presents arithmetic increase, suggests the existence of non-exclusivity of diffusive processes between garnet and biotite inclusion. Hardly, such a small inclusion of biotite (0.1 mm radius) could cause such a significant increase in Fe/(Fe+Mg) in a part of the garnet so far away from the interface (220 μm), even with very low cooling rates. Therefore, it is suggested that garnet may have not maintained equilibrium exclusively with the referred biotite inclusion during an early period of its cooling. This must have been caused by retrograde reaction processes (SPEAR & FLORENCE, 1992; KOHN & SPEAR, 2000) with a large amount of biotite, such as matrix biotite. Modelling performed with similar amounts of garnet and biotite (R_{Garnet} = 1mm; $R_{Biotite}$ = 1mm; $D_{Fe/Mg}^{Biotite} = 100D_{Fe/Mg}^{Garnet}$; T_i = 800°C; Pi = 8 kbar; $Fe/(Fe+Mg)_i^{Garnet} = 0.6261$) at different cooling rates (Fig. 13) show very reasonable adjustment to zones 1 and 2, suggesting initial very high cooling rates (50 to 200°C/Ma), but a pronounced difference to the compositional profile in zone 3.

Thus, migmatite 73A must have had a very complex cooling pattern during which remained in equilibrium with a biotite reservoir such as available matrix biotite (in an early period when biotite was very abundant or when garnet had smaller dimensions than presently) at high cooling rates. This was probably followed by a period when garnet must have been in exclusive equilibrium with its biotite inclusion at lower temperatures. However, the aforementioned cooling pattern, inferred by combining the two modelling with different garnet/biotite volume proportions, cannot simply be put together to infer a coherent cooling pattern, because the

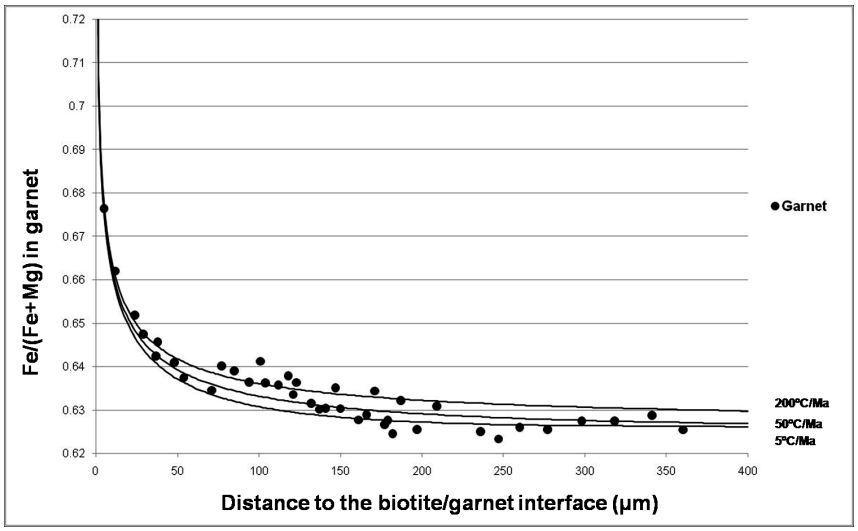

Fig. 12 – Zoned compositional profile of garnet from migmatite 73A (as in Fig. 10) plotted with the different modelling results at different cooling rates, based on the assumption that garnet – biotite inclusion cationic diffusion is exclusive. As can be seen, the GBI profile is only adequate in zone 3, near the biotite inclusion, implying the possibility of having cooling rates as different as 5 and 200ºC/Ma.

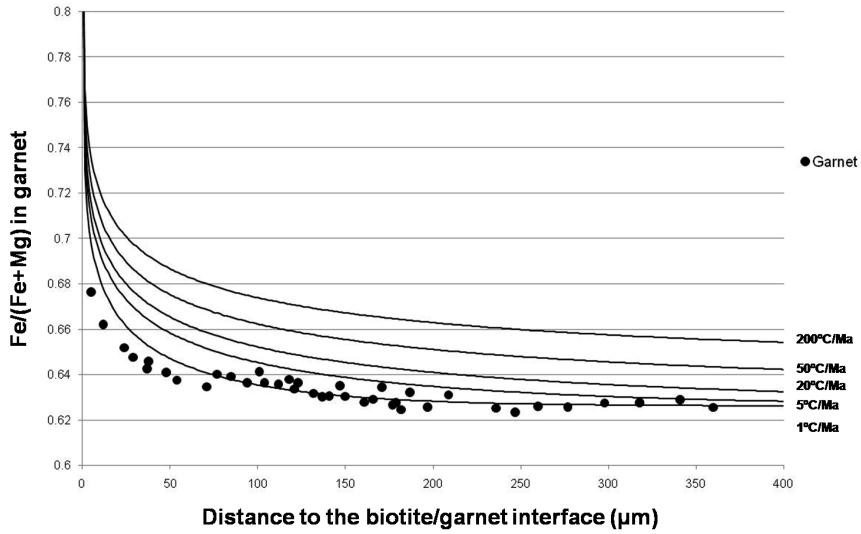

Fig. 13 – Zoned compositional profile of garnet from migmatite 73A (as in Fig. 10) plotted with the different modelling results at different cooling rates, based on the assumption that garnet was in equilibrium with reasonable amounts of matrix biotite. As can be seen, the GBI profile is only adequate to zones 1 and 2 (far from the biotite inclusion) implying very high cooling rates from 50 to 200ºC/Ma.

kinetics of garnet-biotite diffusion of each step is non-reproducible. This was confirmed when several modelling were performed by combining a first non-diffusive (open-system behaviour) followed by a purely diffusive (closed-system behaviour) Fe-Mg exchange between garnet and biotite. No modelling provided reasonable results compatible with the obtained garnet compositional profile near the biotite inclusion.

It can be concluded, after the use of two significantly different methodologies to obtain petrological cooling rates, that there was not exclusivity of mass balanced diffusive processes between the studied garnets and respective biotite inclusions. The system was opened to reaction processes with the rock's matrix, which increases the difficulty of using these methodologies. Therefore, the existence of non-diffusive processes in

garnet, as well as the possibility of plastic deformation of garnet at high temperatures (STOREY & PRIOR, 2005), such as those estimated for peak metamorphic conditions in central RFB (T = 800 – 900°C; BENTO DOS SANTOS, 2008; MUNHÁ *et al*., 2008), makes it very hard to apply this methodologies, since deformation at high temperatures reduces the effective dimension of garnet and allows the interaction between garnet's core and matrix biotite. Probably, this is also the cause for the high dispersion of results in some samples used for the SPEAR & PARRISH (1996) method.

BENTO DOS SANTOS *et al*. (2008) provided thermochronological constraints for the SFSAP sector based on integration of multiple isotopic systems and concluded that migmatites were cooled at relatively stable 3 – 5°C/Ma, whereas granulites were maintained at lower crustal levels and very slowly cooled (< 2°C/Ma) during long-term sub-horizontal transpressive shearing (FONSECA *et al*., 2008). This period of slow-cooling endured until orogenic collapse occurred, leading to abrupt fast cooling of granulites (8 to 30°C/Ma) in the last stages of Brasiliano Orogeny. The present petrological cooling rates are very difficult to interpret and to quantify, but provide qualitative results in agreement with BENTO DOS SANTOS *et al*. (2008) conclusions, such as the idea of having high temperature maintenance that reequilibrated the garnets, followed by very fast cooling that did not allow significant Fe/Mg diffusion between garnet and biotite inclusions.

Intense deformation caused by the long-term sub-horizontal transpressive shearing (FONSECA *et al*., 2008) can be seen in sheared migmatites and granulites (as described in the Petrography section of this work), as well as in the fact that some are abundantly blastomylonitized. This is the probable cause for the open-system behaviour found in some samples. It may have altered biotite diffusion mechanisms and reequilibrated garnet with minerals or fluids outside the garnet – biotite inclusion system, adding complexities and increasing the uncertainties regarding the use of these methodologies.

7. CONCLUSIONS

The several obtained petrological cooling rates with two significantly different methodologies are very dubious and provide mainly qualitative results due to the complex evolution of the belt that allowed open-system behaviour. This altered biotite diffusion mechanisms or reequilibrated garnet with minerals or fluids outside the garnet – biotite inclusion system. Nevertheless, the presented results, although very difficult to interpret and to quantify, provide qualitative results that are in broad agreement with previously obtained geochronological cooling rates. Thermochronology based on integration of multiple isotopic systems are thus more accurate for inferring cooling rates in rocks that endured complex cooling patterns, significant deformation and Fe-Mg open-system behaviour.

ACKNOWLEDGEMENTS

FAPESP, POCA-PETROLOG (CEGUL, UI: 263; POCTI/FEDER), GEODYN (POCTI – ISFL – 5 – 32) and a PhD scholarship from FCT (SFRH/BD/17014/2004) co-financed by FEDER provided support for field and analytical work. Teresa Palácios and Octávio Chaveiro are gratefully acknowledged for long-term logistic and moral support. The authors are also grateful for the comments and suggestions of two anonymous reviewers that greatly added to the improvement of this work.

REFERENCES

BASCOU, J., RAPOSO, M., VAUCHEZ, A., EGYDIO-SILVA, M. (2002) – Titanohematite lattice preferred orientation and magnetic anisotropy in high temperature mylonites. *Earth and Planetary Science Letters*, **198**, 77-92.

BENTO DOS SANTOS, T. (2008) – Petrologia e termocronologia de granulitos no sector central da Faixa Ribeira (Regi‹o de São Fidelis, Rio de Janeiro, Brasil). *Unpublished Ph.D. thesis*, University of Lisbon, Lisbon, 388.

BENTO DOS SANTOS, T., MUNHÁ, J., TASSINARI, C., FONSECA, P., DIAS NETO, C. (2007) – Thermochronological evidence for long-term elevated geothermal gradients in Ribeira Belt, SE Brazil. *Geochimica et Cosmochimica Acta*, **71**, 15, 1, A79.

BENTO DOS SANTOS, T., FONSECA, P., MUNHÁ, J., TASSINARI, C., DIAS NETO, C. (2008) – Structural and thermochronological constrains on the tectonic evolution of Ribeira Belt, SE Brazil. *Geophysical Research Abstracts*, **10**, A-00261.

CAMPOS NETO, M., FIGUEIREDO, M. (1995) – The Rio Doce orogeny, Southeastern Brazil. *Journal of South American Earth Sciences*, **8**, 2, 143-162.

CHAKRABORTY, S., GANGULLY, J. (1992) – Cation diffusion in aluminosilicate garnets – experimental determination in spessartine-almandine diffusion couples, evaluation of effective binary diffusion coefficients, and applications. *Contributions to Mineralogy and Petrology*, **111**, 74-86.

CORDANI, U. (1971) – Síntese da geocronologia Pré-Cambriana da região costeira atlântica meridional da América do Sul. *25th Congresso Brasileiro de Geologia (Extended Abstract)*, São Paulo, 179-180.

Cordani, U., Delhal, J., Ledent, D. (1973) – Orogenéses superposées dans le Précambrien du Brésil sud-oriental (États de Rio de Janeiro et de Minas Gerais). *Revista Brasileira de Geociências*, **3**, 1-22.

Dodson, M. (1973) – Closure temperature in cooling geochronological and petrological systems. *Contributions to Mineralogy and Petrology*, **40**, 3, 259-274.

Ehlers, K., Powell, R., Stuwe, K. (1994) – The determination of cooling rate histories from garnet-biotite equilibrium. *American Mineralogist*, **79**, 737-744.

Ferry, J., Spear, F. (1978) – Experimental calibration of the partioning of Fe and Mg between biotite and garnet. *Contributions to Mineralogy and Petrology*, **66**, 113-117.

Fonseca, P., Bento dos Santos, T., Munhá, J., Tassinari, C., Dias Neto, C. (2008) – Thermochronological and structural analysis of the geodynamic evolution of Ribeira Belt, SE Brazil. *Geochimica et Cosmochimica Acta*, **72**, 12, 1, A276.

Gangully, J., Cheng, W., Chakraborty, S. (1998) – Cation diffusion in aluminosilicate garnets: experimental determination in pyrope-almandine diffusion couples. *Contributions to Mineralogy and Petrology*, **131**, 171-180.

Heilbron M., Machado, N. (2003) – Timing of Terrane Accretion in the Neoproterozoic-Eopaleozoic Ribeira Orogen SE Brazil. *Precambrian Research*, **125**, 87-112.

Heilbron, M., Valeriano, C., Tupinambá, M., Almeida, J., Valadares, C., Silva, L., Nva, D., Dios, F. (1993) – Compartimentação tectónica e evolução geológica do segmento central da Faixa Ribeira, a Sul do Cráton do São Francisco. *II Simpósio do CSF (Extended Abstract)*, Salvador, 263-265.

Kohn, M., Spear, F. (2000) – Retrograde Net Transfer Reaction (ReNTR) Insurance for P-T estimates. *Geology*, **28**, 1127-1130.

Lasaga, A., Richardson, S., Holland, H. (1977) – The mathematics of cation diffusion and exchange between silicate minerals during retrograde metamorphism. In: Saxena, S. K., Battacharji, S. (Eds.) *Energetics of Geological Processes*, 354-387.

Machado, N., Valladares, C., Heilbron, M., Valeriano, C. (1996) – U-Pb geochronology of the central Ribeira belt Brazil and implications for the evolution of the Brazilian Orogeny. *Precambrian Research*, **79**, 347-361.

Munhá, J., Bento dos Santos, T., Tassinari, C., Fonseca, P. (2008) – Pseudosection and thermobarometry constraints on the P-T-t evolution of Ribeira Belt, SE Brazil. *Geochimica et Cosmochimica Acta*, **72**, 12, 1, A664.

Munhá, J., Cordani, U. G., Tassinari, C., Palácios, T. (2005) – Petrologia e Termocronologia de gnaisses migmatíticos da Faixa de Dobramentos Araçuaí, Espírito Santo, Brasil. *Revista Brasileira de Geociências*, **35**, 1, 123-134.

Pedrosa Soares, A., Noce, C., Wiedmann, C., Pinto, C. (2001) – The Araçuai-West Congo Orogen in Brazil: an overview of a confined orogen formed during Gondwanaland assembly. *Precambrian Research*, **110**, 307-323.

Pedrosa-Soares, A., Wiedemann-Leonardos, C. (2000) – Evolution of the Araçuai Belt and its connection to the Ribeira Belt, Eastern Brazil. In: Cordani, U., Milani, E., Thomaz-Filho, A. and Campos, D.A (Eds.), *Tectonic Evolution of South America*. Rio de Janeiro, 265-285.

Powell, R., Holland, T. (1999) – Relating formulations of the thermodynamics of mineral solid solutions: Activity modelling pyroxenes, amphiboles and micas. *American Mineralogist*, **84**, 1-14.

Schmitt, R., Trouw, R., Medeiros, S., Dantas, E. (2008) – Age and geotectonic setting of Late Neoproterozoic juvenile mafic gneisses and associated paragneisses from the Ribeira Belt (SE Brazil) based on geochemistry and Sm – Nd data – Implications on Gondwana assembly. *Gondwana Research*, **13**, 4, 502-515.

Schmitt, R., Trouw, R., Schmus, W., Pimentel, M. (2004) – Late amalgamation in the central part of West Gondwana: new geochronological data and the characterization of a Cambrian collision orogeny in the Ribeira Belt (SE Brazil). *Precambrian Research*, **133**, 29-61.

Spear, F., Florence, F. (1992) – Thermobarometry in granulites: Pitfalls and new approach. *Precambrian Research*, **55**, 209-241.

Spear, F., Parrish, R. (1996) – Petrology and cooling rates of the Valhalla Complex, British Columbia, Canada. *Journal of Petrology*, **37**, 733-765.

Storey, C., Prior, D. (2005) – Plastic deformation and recrystallization of garnet: a mechanism to facilitate diffusion creep. *Journal of Petrology*, **46**, 12, 2593-2613.

Storm, L., Spear, F. (2005) – Pressure, temperature and cooling rates of granulite facies migmatitic pelites from the southern Adirondack Highlands, New York. *Journal of Metamorphic Geology*, **23**, 107-130.

Trouw, R., Heilbron, M., Ribeiro, A., Paciullo, F., Valeriano, C., Almeida, J., Tupinambá, M., Andreis, R. (2000) – The central segment of the Ribeira Belt. In: Cordani, U.G., Milani, E.J., Thomaz-Filho, A. and Campos, D.A (eds.), *Tectonic Evolution of South America*. Rio de Janeiro, 297-310.

Tupinambá, M. (1999) – Evolução tectônica e magmática da Faixa Ribeira na região serrana do Estado do Rio de Janeiro. *Unpublished Ph.D. thesis*, University of São Paulo, São Paulo, 236.

Valladares, C., Machado, N., Heilbron, M., Duarte, B., Gauthier, G. (2008) – Sedimentary provenance in the central Ribeira belt based on laser-ablation ICPMS $^{207}Pb/^{206}Pb$ zircon ages. *Gondwana Research*, **13**, 4, 516-526.

Vauchez, A., Tommasi, A., Egydio-Silva, M. (1994) – Self-indentation of a heterogeneous continental lithosphere. Geology, **22**, 967-970.

Wimmenauer, W., Brynhi, I. (2007) – 6. Migmatites and related rocks. A proposal on behalf of the IUGS Subcommission on the Systematics of Metamorphic Rocks. Web Version of 01.02.07, 1-5 (http://www.bgs.ac.uk/scmr/docs/papers/paper_6.pdf).

Artigo recebido em Julho de 2009
Aceite em Outubro de 2009